Preparation of rhodium nano-particles using microwaves

M. Ugalde, E. Chavira, L.A. Figueroa, C. Quintanar, F. Espinosa-Magaña, E.A. Zaragoza-Contreras, M.T. Ochoa Lara.

Abstract

A new process for synthesizing rhodium (Rh) nano-particles by sol–gel processing using acrylamide and microwaves is reported and discussed. Three heat treatments were applied: the first required the use of microwaves, with an inert gas (Ar) flux, to decompose the organic material; the second and third treatments, respectively, were carried out into a furnace in air at temperatures of 600 and 1,000 °C. This procedure ensured the removal of by-products produced during the sol–gel reaction. The synthesis of a pure nano-Rh was confirmed by X-ray diffraction (XRD), where the presence of a cubic structure was observed (PDF file 089-7383), and EDX. Thermogravimetric analysis (TGA), in addition to determining the decomposition temperatures, enabled the heat treatment conditions needed to obtain pure nano- Rh to be elucidated. Furthermore, the morphology was observed with a scanning electron microscope (SEM). After the heat treatment at 1,000 °C, SEM images showed grain sizes between 3 and 200 nm. High-resolution transmission electron microscopy (HR-TEM) confirmed the production of those nano- particles, and the beginning of the formation of clusters as a consequence of the high temperature applied to the system.

Keywords: Sol-gel method, Rhodium nanoparticles, SEM, HR-TEM, TGA, DRX.

Introduction

Transition metals have gained importance because of their particular properties, i.e., their partially filled d subshell allows the d-block metals to have multiple oxidation numbers. Because of this, transition metal nanotechnology offers a number of applications; consequently, the creation of new synthetic methods is of great interest. In particular, the scientific community is interested in finding new ways of synthesizing rhodium (Rh) nano-crystals because they present a wide range of applications; for instance, hydrogenation of unsaturated compounds [1], hydrogenolysis reaction [2], oxidation [3], and C–C coupling reactions [4]. Rh nanoparticles also play an important role in sensing of biological molecules [5–7].

As is well known, many metallic nano-crystals have been prepared by various methods. Of these, chemical synthesis methods appear to offer advantages over physical methods for controlling particle size. Chemical methods may be used to control the growth of the metal nanoparticles in a solution by (for example) the reduction of appropriate metal precursors in the presence of acids when varying the pH [8].

The sol–gel method allows nanometer-sized metal particles to be synthesized using lower temperatures [9] with a single heat treatment, in contrast to solid-state reactions, which require constant monitoring of the X-ray technique to define the heat treatments needed to generate the desired phase. Therefore, the sol–gel method is advantageous because it allows a better control of the pore size distribution, thermal stability, homogeneity and purity of the materials produced.

Microwaves will generally heat any material that contains mobile electric charges, such as polar molecules in a solvent or conducting ions in a solid [10]. Microwave

heating has shown to reduce dramatically the reaction times and to enhance the purity of the material produced. This behavior is attributed to the reduction of unwanted side reactions when compared to conventional heating methods. According to Patel et al. [11] the main characteristic of this process is the uniformity of heating, and this property may result in a narrow distribution of particle sizes. Vollmer et al. [12] reported that it was possible to produce transition metal nanoparticles, through microwave heating, by precipitation from Ionic Liquids. They concluded that no stabilizers or capping molecules were needed to produce small and uniform metal particles.

The objective of this work is to produce Rh nano- particles using a modified sol–gel technique coupled with microwave processing to decompose the precursor and generate the final product.

Experimental procedure

Materials: The reagents used in this work were: Rhodium metal (99.9 %, Sigma-Aldrich), ammonium hydroxide (28–30 %, J. T. Baker), and sulfuric acid (J. T. Baker), ethylenediaminetetraacetic acid (99 %, Fluka), N,N'-Methylenebisacrylamide (99.5 %, Fluka), 2,2'-azobis(2-methylpropionamidine) dihydrochloride (98 %, Fluka), acrylamide monomer (99 %, Sigma-Aldrich), and distilled water.

Nanoparticles: The synthesis of Rh nano- particles was carried out using the sol–gel method, and acrylamide polymerization [13]. Initially 439 mmol of Rh metal were dissolved in sulfuric acid and distilled water (80 mL) at 70 °C, forming a yellowish solution. Later, the solution was cooled down to ambient temperature prior to adjusting the pH ca. to 7 by adding ammonium hydroxyde (NH_4OH), following the method

outlined in [14]. As soon as a pH ca. 7 was reached, the solution was heated up to 80 °C, and 51.6 mmol of ethylenediaminetetraacetic acid (EDTA) was added to complex the rhodium ions, avoiding the formation of agglomerates. After this, 211 mmol of acrylamide monomer and 9.72 mmol of crosslinking agent, *N,N'*-Methylenebisacrylamide were added to the initial solution. Finally, 5.5 mmol of initiator, 2,2'-azobis(2-methylpropionamidine)dihydrochloride, were added to launch polymerization to produce the gel [15]. The pH of the solution was constantly monitored by means of a pH meter (Thermo Scientific Orion star A221). The polymerization was performed at 80 °C. It is worth noting that all the processes were done under air atmosphere. In neutral or basic conditions, the time required to form the gel decreases considerably [16].

The resulting gel was placed in a microwave and slowly decomposed by heating from 80 to 170 °C, under argon atmosphere for 30 min. The product, a xerogel, was obtained which was pulverized immediately using an agate mortar. Finally, heat treatments at 600 and 1,000 ± 4 °C, for 2 h under air atmosphere, were applied.

Characterization: The crystal structure was determined through XRD, using a Panalytical X0Pert PRO MPD diffractometer, with Cu Kα radiation (λ = 1.5406 Å´) operated at 40 kV and at 35 mA. The diffractometer was equipped with an X0Celerator, mark 20 detector. The XRD patterns were collected at room temperature over the 2θ range of 10° to 70°, with a step size of 0.0167° and a time per step of 30 s.

A thermal analyzer (STD Q600, TA-Instruments) using a standard, alumina pan, with a heating rate of 10 °C min-1 in air atmosphere, over a range of temperatures of 30–1,000 °C was used to study decomposition temperatures.

The microstructure and morphology were observed using a scanning electron microscope (SEM JSM5800L, JEOL) and a high-resolution transmission electron microscope (HRTEM JEM-2200FS, JEOL). The samples were prepared by dispersing ca. 2 mg of Rh nano-crystals in 4 mL of 1-propanol, and were then sonicated for 15 min. Finally, a drop of dispersion was deposited on a lacey carbon supported copper grid (200 mesh). A series of SEM micrographs, at 10 kV, and HR-TEM, at 200 kV, were taken. The composition of the material was determined with an Energy Dispersive X-Ray (EDX) spectroscope, with an Oxford Incax-sight 7688 detector.

The size distribution was determined from the micrographs taken with the HRTEM. The size distributions histograms were calculated using ‘‘Image J’’ software (Image Processing and Analysis in Java). In this work, the diameters of at least 100 particles were measured and mean values determined. The statistical error was also included.

Fourier Transform Infrared analysis (FT-IR) was carried out with a ThermoScientific Nicolet 6700 spectrometer equipped with a ‘‘Smart iTR diamond accessory’’. The measuring resolution was 2 cm^{-1} and 256 spectra were co-added in the range of 600–4,000 cm^{-1}.

Results and discussion

Figure 1a shows the xerogel product obtained after being pulverized. As can be seen in the figure, a non-homogeneous agglomerate distribution is observed due to the material being rather hard, making it difficult to pulverize prior to calcination. Figure 1b illustrates the resulting material after the heat treatment at 1,000 °C in air for 2 h. After increasing the temperature, a change of color was observed in the resulting material. This color change indicates the formation of Rh and the loss of organic by-products formed during the sol–gel reaction. When this organic material is subjected to a heat treatment above 600 °C, it decomposes forming CO and CO_2, as observed by XRD and TGA (this will be presented and discussed in the following section). It is worth noting the small final amount of Rh obtained when compered to the initial amount of xerogel processed. The reaction yield for this experimental method was around 30 %.

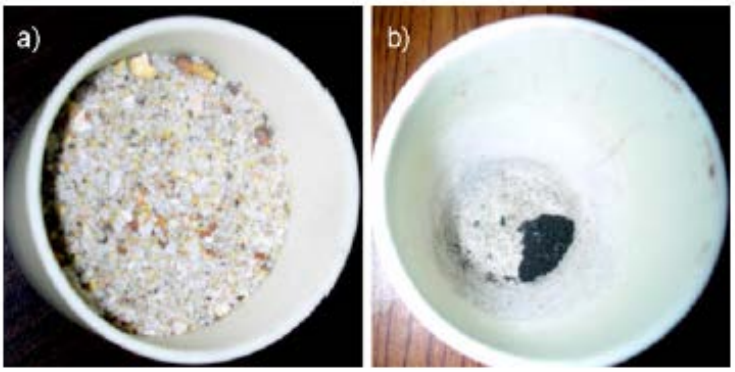

Fig. 1 a xerogel and b the material after heat treatment at 1,000 °C

X Ray diffraction: The X-ray diffractograms have enabled the compounds formed during the sol–gel reaction to be identified, and the changes undergone by the material to be investigated. The gel and xerogel diffractograms (Fig. 2a) showed the presence of ammonium sulfate ($(NH_4)_2SO_4$) (PDF 76-0579) with an orthorhombic structure, which

was presumably formed during the addition of NH_4OH. However, the gel would be expected to have an amorphous structure due to the presence of the amorphous polymer in which the Rh ions and cluster are encapsulated.

Figure 2b shows the XRD pattern of the material heattreated at 600 °C, with the presence of Rh oxide (Rh_2O_3), corresponding to a rhombohedral structure (PDF file 43-0009), and traces of $Rh_2(SO_4)_2$ (PDF file 30-1038) and RhO(OH) (PDF file 27-1383) clearly observed. Figure 2b also shows the line patterns obtained for the material after treatment at 1,000 °C. Here, after increasing the temperature up to 1,000 °C, pure Rh metal is generated and the aforementioned impurities are then removed. The peaks for the pure Rh phase occurred at 2h = 41.028, 47.78 and 69.8° and correspond to a cubic structure (PDF file 089-7383).

The reduction of theRh_2O_3 could be attributed to twomain factors: (a) As mentioned above, since the xerogel is formed by organicmaterial, after the heat treatments the formation of CO may be partially responsible for reducing the Rh_2O_3 and (b) thermodynamically, the Rh_2O_3 is unstable above 1,000 ± 30 °C, where an irreversible thermal dissociation, according to the following scheme, has been observed [17].

$$\beta - Rh_2O_3 \xrightarrow[1{,}000\,^{\circ}C]{\Delta} 2Rh + {}^{3}/_{2}O_2$$

Thermogravimetric analysis: TGA enables the temperatures at which the material should be treated in order to obtain the Rh metal and to promote the removal of the by-products and the organic matter generated during the sol–gel reaction to be identified,

as shown in Fig. 3. Table 1 summarizes the results obtained by the TGA analysis. The TGA traces showed that at 230 and 241 °C the thermal degradation of poly(acrylamide) and EDTA started. The thermograms also showed that the $(NH_4)_2SO_4$ disappeared within the range 510–523 °C, while between 597 and 620 °C the formation of Rh_2O_3 was observed. The gel and the xerogel exhibited similar trends.

Finally, to eliminate by-products and oxides formed during heat treatment, the system was heated up to 1,000 °C. After this process, pure Rh metal was obtained, confirming the XRD results shown in Fig. 2b. The weight losses were in agreement with the quantities of the material used during the synthesis.

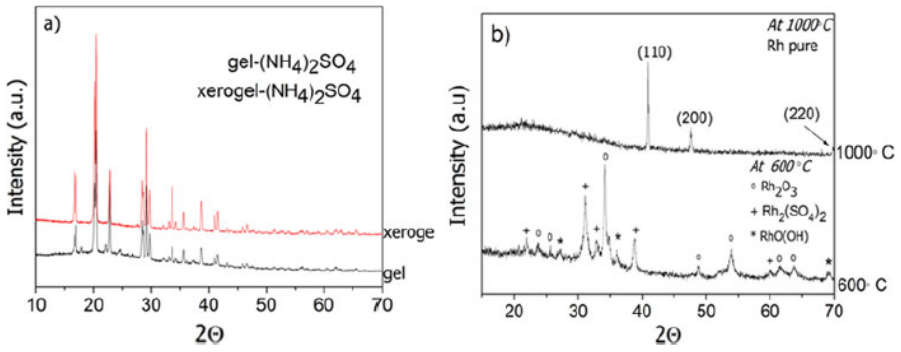

Fig. 2 **a** X-ray diffraction for the gel and xerogel, **b** X-ray diffraction after the heat treatment from 600 to 1,000 °C

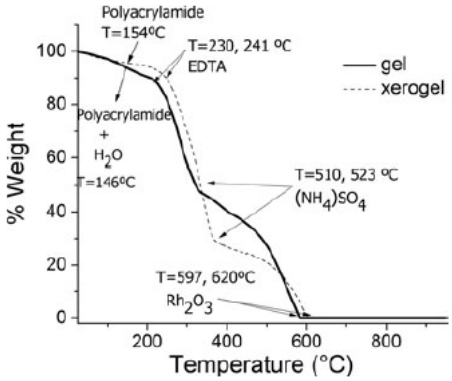

Fig. 3 TGA curves for the gel and xerogel

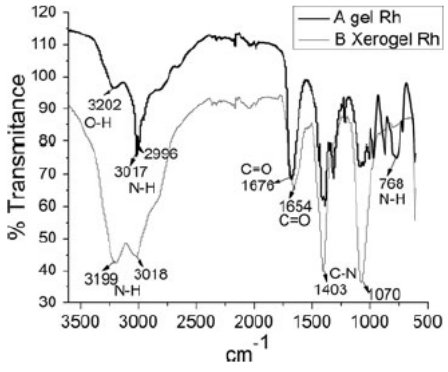

Fig. 4 *Spectrum a* FT-IR from the gel and *spectrum b* FT-IR from the xerogel

Table 1 Thermal transitions for the gel and xerogel

Thermal transitions	Gel Temperature (°C)	Xerogel Temperature (°C)	Weight loss gel (%)	Weight loss xerogel (%)
Water	80	–	4	–
Removal of the polymer (acrylamide) and EDTA	241	230	13	9
Elimination of $(NH_4)_2SO_4$ compound	523	510	76	82
Rh_2O_3 formation	620	597	99	99

FTIR analysis: The FT-IR analysis is shown in Fig. 4. The following signals are observed in spectrum A (gel): the band at 3,202 cm^{-1} was ascribed to the antisymmetric stretching vibrations of N–H bond of amide groups; the bands at 3,018 and 2,996 cm^{-1} correspond, respectively, to the vibrations of C–H bond of = CH and to the symmetrical vibration of C–H bond of H_2C = , which indicates that acrylamide monomer did not polymerize completely during crosslinking; the signal at 1,651 cm^{-1} was assigned to the stretching vibration of C = O of amide bonds; the peak in the region of 1,403 cm^{-1} was attributed to the stretching vibration of C–N bonds, and the band at 768 cm^{-1} can be assigned as the out-of-plane wagging of N–H bond of primary amides. Additionally, the bands at 1,310 and 1,080 cm-1 ascribed to stretching vibrations of C–N bonds of tertiary amines are an indication of the presence of EDTA salt.

Spectrum B shows the material after the microwave treatment (xerogel). As expected, after this treatment, the gel suffered degradation; consequently, several absorption bands observed in spectrum A have disappeared. The bands at 3,187, 1,654, and 1,403 cm^{-1} indicate, respectively, the remnants of N–H, C = O, and C–N bonds of amides. The band at 3,018 cm-1 indicate that = CH (insaturations) are still

present, and similarly, the band at 1,070 cm^{-1} (C–N bonds) indicates that EDTA still remains.

SEM analysis: SEM micrographs showed the morphology of the material after the heat treatments. At 600 °C, the material displayed a morphology based on two kinds of particles: a dispersion of spherical granules of sizes between 5 and 10 nm, and larger granules ranging from 60 to 90 nm, as shown in Fig. 5a. After increasing the temperature up to 1,000 °C, the sintering process in the material started as observed in Fig. 5b. The material exhibit elongated shapes with sizes ranging from 100 to 200 nm.

Tem analysis: The HRTEM analysis confirmed that when the temperature increases during the synthesis, the coalescence of particles occurred, forming large clusters of ~200 nm, as shown in the SEM images. It is worth noting that, in order to observe such particles by HRTEM, the clusters were dispersed by ultrasonication. With this process, nano-particles of rhodium with different spherical and elongated particle shapes, with an average size of 3 nm, were obtained, as shown in Fig. 6.

Figure 7 shows the dark field and bright field HRTEM micrographs of the nano-particles of Rh. These figures clearly show the dispersion of the clusters after the sonication process, resulting in the formation of the nanoparticles of pure metallic Rh.

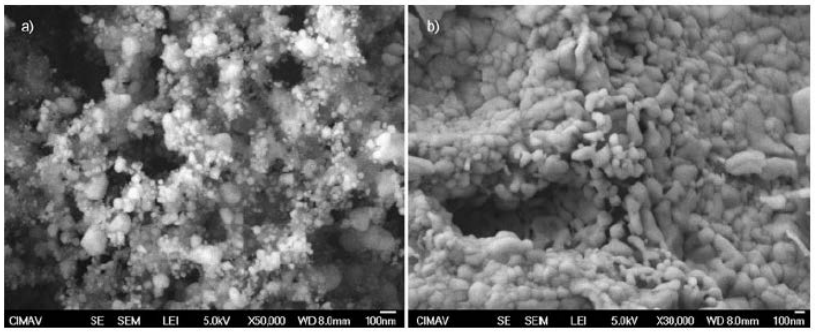

Fig. 5 SEM Micrographs of the material heat-treated at: **a** 600 °C and **b** 1,000 °C

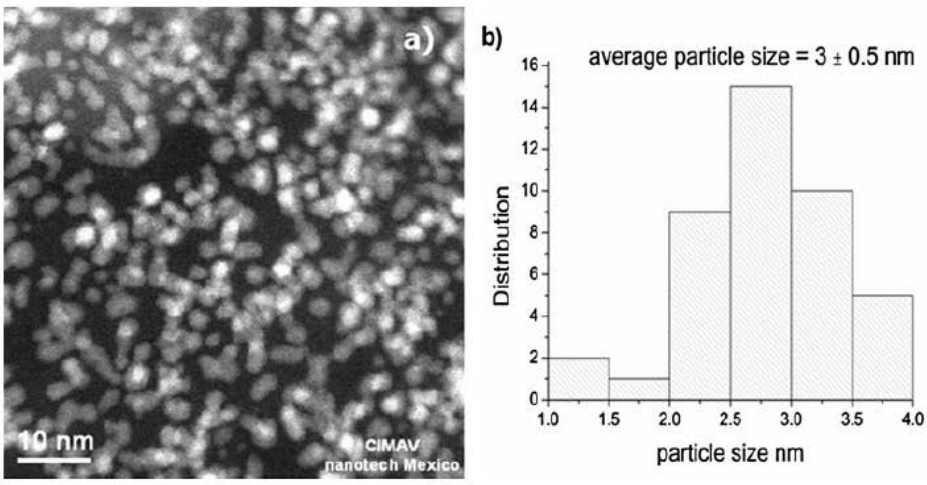

Fig. 6 a TEM dark field image at 1,000 °C and b Particle size distribution of Rh nanoparticles

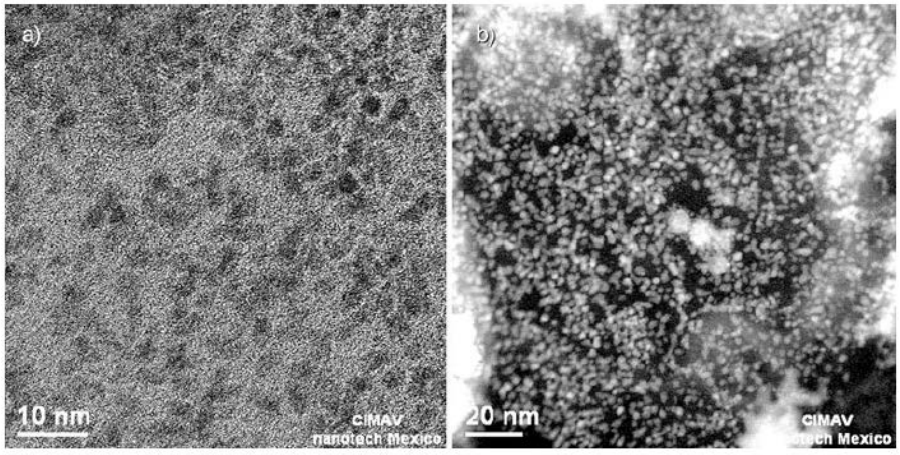

Fig. 7 a Bright field and b dark field HRTEM Micrographs, of the same nano-Rh heat treated at 1,000 °C

Figure 8 shows the EDX for the Rh nano-particles, where the peaks of Rh are clearly observed. The C and Cu peaks are due to the carbon-coated copper grid used for HRTEM measurements. This analysis would suggest the absence of impurities such as sulphur (S), that might come from the $(NH_4)_2$ SO4 compound, that was formed during the synthesis.

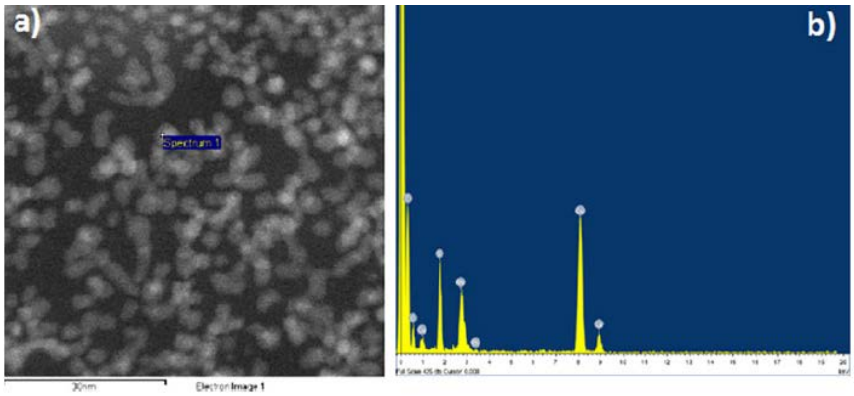

Fig. 8 a HRTEM Micrograph of nano-Rh heat treated at 1,000 °C and b corresponding EDX data

Different methods have been developed to produce metal nanoparticles, but these differ significantly, depending on the application required. Mu et al. [18] stabilized Rh particles using the ionic (poly [(N-Vinyl-2-pyrrolidone)- co-(1-vinyl-3-alkylimidazoliumhalide) copolymer in ionic solvents. They found a distribution of particles of ~3 ± 0.6 nm. These nanoparticles were used as catalysts for arene hydrogenation. Similarly, Ashida et al. [19], produced Rh nanoparticles through chemical reduction. This synthesis method is widely used to produce nanoparticles, which will be used as catalysts, on an industrial scale. They reported that the Rh nanoparticles are formed by reducing Rh ions in ethanol–water solvent with the polymers of polyvinylpyrrolidone (PVP) [20, 21]. The PVP encapsulates the nanoparticles in the solution and prevent their aggregation. The growth of the nanoparticles may be limited during the reduction by the space restrictions imposed by the three-dimensional PVP network. The particles generated from this method showed an average size of 3.2 ± 0.7 nm. However, it was noted that within the network of the Rh-PVP, there were Cl atoms. These species came from the reagent used ($RhCl_3$

($_3H_2O$)). During the synthesis, the Cl atoms were entrapped as an impurity in the inter-lattice planes of the material.

The reported aforementioned methods have some disadvantages. In particular, the particles produced can only be used for catalysis, since they are stabilized by another material. In addition, the impurities anchored in the structure may detrimentally affect their catalytic properties. In the present case, although the particle sizes are very similar to those obtained with the standard reported sol–gel methods, our particles are not restricted to a single application, as the resulting Rh metal was found to be free of impurities. In this work, the stabilizer used (EDTA) is completely removed with the heat treatment. The purity of this material is of great importance for applications in other areas such as: magnetic [22], optical [23] or sensors [24].

Notwithstanding the fact that the total experimental process time was slightly longer than those reported in the literature, the resulting material was found to have higher purity when compared with those reported previously, where additional phases of impurities by XRD and EDX were found.

Conclusions

The proposed microwave-assisted, sol–gel method was able to obtain pure Rh nano-particles with an average size ~3 nm. The TGA performed on the material allowed us to find the decomposition temperatures needed to obtain the pure material. With the aim of removing the by-products and oxides formed during the heat treatment, the system was heated to 1,000 °C. After this process, pure metal Rh was obtained. A highly pure metallic Rh was confirmed by X-ray diffraction (XRD) and EDX. The

morphology observed by SEM showed the formation of clusters of ~200 nm. The clusters were successfully dispersed with an ultrasonic cleaner. The HRTEM analysis confirmed the production of nano-particles of ~3 nm.

Acknowledgments

This work was supported by PAPIIT IN116912 project. M. Ugalde acknowledges financial support from CONACyT through scholarship 207277. The authors express their grateful acknowledgment to Adriana Tejeda, Enrique Torres Moye, Carlos Elías Ornelas Gutie´rrez and Wilbert Antu´nez for their technical support and discussions. The authors also thank the referees for their helpful and constructive comments. IAF acknowledges the financial support from PAPIIT-UNAM through project IB100712. Laboratorio Nacional de Nanotecnología, Centro de Investigación en Materiales Avanzados, S.C., Ave. Miguel de Cervantes #120, C.P. 31109, Chihuahua, Chih., México is also acknowledged.

References

1. Robert F, Oehme G, Grassert I, Sinou D (2000) J Mol Catal A 156:127–132
2. Mizuno T, Matsumura Y, Nakajima T, Mishima S (2003) Int J Hydrogen Energy 28:1393–1399
3. Gniewek A, Trzeciak AM, Ziołkowski JJ, Kepinski L, Wrzyszcz J, Tylus W (2005) J Catal 229:332–343
4. Narayanan R, El-Sayed MA (2004) J Phys Chem B 108:8572–8580

5. Shumyantseva VV, Carrara S, Bavastrello V, Riley DJ, Bulko TV, Skryabin KG, Archakov AI, Nicolini C (2005) Biosens Biolectron 21:217–222

6. Willner I, Baron R, Willner B (2007) Biosens Bioelectron 22:1841–1852

7. Zapiter JMD, Tissue BM, Brewer KJ (2008) Inorg Chem Commun 11:51–56

8. Nalwa HS (2000) Handbook of nanostructured materials and nanotechnology. Academic Press, California

9. Harada M, Abe D, Kimura Y (2005) J Coll Inter Sci 292:113–121

10. Glaspell G, Lindsay Fuoco M, El-Shall S (2005) J Phys Chem B 37:17350–17355

11. Patel K, Kapoor S, Dave DP, Mukherjee T (2005) J Chem Sci 117:311–316

12. Vollmer C, Redel E, Abu-Shandi K, Thomann R, Manyar H, Hardacre C, Janiak C (2010) Chem Eur J 16:3849–3858

13. Ugalde M, Chavira E, Ochoa-Lara MT, Quintanar C (2011) J Nano Res 14:93–103

14. Sin A, Odier P (2000) Adv Mater 12:649–652

15. Jiménez-Mier J, Herrera G, Chavira E, Ban˜os L, Guzma´n J, Flores C (2008) J Sol-Gel Sci Technol 46:1–10

16. Gonzalez RD, Lopez T, Gomez R (1997) Catal Today 35:293–317

17. Skrobot VN, Ugolkov VL, Grebenshchikov RG, Gusarov Subsolidus VV (2005) Inorg Mater 41:840–844

18. Mu XD, Meng JQ, Li ZC, Kou Y (2005) J Am Chem Soc 127:9694–9695

19. Ashida T, Miura K, Nomoto T, Yagi S, Sumida H, Kutluk G, Soda K, Namatame H, Taniguchi CM (2007) Surface Sci 601:3898–3901

20. Huang Y, Chen J, Min L, Chen H, Li R, Li Y, Li X (2001) J Mol Catal A 170:143–146

21. Pellegatta J-L, Blandy C, Colliere V, Choukroun R, Chaudret B, Cheng P, Philippot K (2002) J Mol Catal A 178:55–61

22. Morneta S, Vasseura S, Grassteb F, Veverkac P, Goglioa G, Demourguesa A, Portiera J, Pollertc E, Duguet E (2006) Prog Solid State Chem 34:237–247

23. Alivisatos AP (1996) Science 271:933–937

24. Kreibig U, Vollmer M (1994) Optical properties of small metal clusters. Springer, Berlin